Revision 1

Hydrogen incorporation in crystalline zircon: insight from *ab initio* calculations

Sanda M. Botis[1], Yuanming Pan[2], Rodney C. Ewing[1]

[1]Department of Earth and Environmental Sciences, University of Michigan, Ann Arbor, Michigan 48109-1005, U.S.A.

[2]Department of Geological Sciences, University of Saskatchewan, Saskatoon, SK, S7N 5E2, Canada

ABSTRACT

The OH stretching vibration frequencies of crystalline zircon that contains water have been investigated by quantum mechanical calculation using CRYSTAL09 and several hybrid functionals. Incorporation mechanisms considered for H in zircon include: *i*) hydrogarnet and partial hydrogarnet-type substitution, *ii*) H-compensated trivalent substitution at the Si site and *iii*) H-compensated trivalent substitution at the Zr site. The results provide a clear picture of the H locations in zircon and their associated IR stretching vibrations. Based on the results of structural relaxation and corresponding OH stretching calculations, we can assign the 3420 cm^{-1} band to a hydrogarnet or partial hydrogarnet type-substitution with polarization dependent on the extent of local relaxation (i.e., closer to E//c for partial hydrogarnet and less polarized for hydrogarnet). These results also show that the 3385 cm^{-1}(E⊥c) IR band originates from H incorporation that accompanies a trivalent cation substitution at the Si-site. As an example of such a substitution, the [AlO_4/H] defect was investigated. H-incorporation coupled with a trivalent cation substitution at the Zr-site appears to be responsible for generating the 3180 cm^{-1}(E⊥c) IR band. The *ab initio* calculation on [YO_8/H] and [LaO_8/H] structures show that the

3180 cm^{-1} band represents an average between two distinct bands at ~3220-3250 cm^{-1} and ~ 3100 cm^{-1} attributed to H locations close to or further away from the Zr-substituted atom. The energetics of these substitutions demonstrate that the overlapping of the two IR bands depends on the substituting cation, and this is controlled, in part, by the thermal history of the sample and/or by the experimental conditions under which the IR spectra are obtained. Furthermore, these results predict for the first time the existence of a peroxy-type O bond associated with the partial hydrogarnet substitution in the zircon structure that now accounts for the ~800 cm^{-1} bands.

Keywords: hydroxyl, zircon, infrared, ab initio, DFT.

INTRODUCTION

Zircon is aubiquitous accessory mineral that is used as a geochemical tracer, geochronometer and geobarometer in reconstructing Earth's crustal evolution. Furthermore, because zircon can incorporate heavy lanthanides and actinides (Spear 1980; Hoskin and Schaltegger 2003) and is chemically durable, it has been proposed as a crystalline nuclear waste form (Ewing, 1999; Ewing 2001 and references therein).

Despite the anhydrous nature of zircon and its exceptional durability under diverse geochemical conditions, a number of studies have reported a hydrous component in natural zircon (Frondel 1953; Frondel and Collete 1957; Coleman and Erd 1961; Mumpton and Roy 1961; Krstanovic 1964; Caruba et al. 1985) and especially in samples that have experienced radiation-induced amorphization (Aines and Rossman 1986; Woodhead et al. 1991; Nasdala et al. 2001, Salje and Zhang 2006; Zhang et al. 2010). From a geochemical perspective, the incorporation of water into zircon, as bonded hydroxyl groups, could play an essential role in

controlling the partitioning mechanism and degree of incorporation of M^{3+}cations (i.e., Y^{3+}, REE^{3+}) when the P^{5+} content is insufficient to attain charge balance through a xenotime substitution mechanism (Hinton et al. 2003). From the perspective of nuclear waste form performance, understanding the interaction of zircon with water is crucially important in predicting its susceptibility to alteration and dissolution over long periods (Salje and Zhang 2006, Delattre et al. 2007). Thus, the exact location of H in the crystalline structure of zircon is essential to understanding the incorporation mechanisms for trace elements and the role of hydration in the metamictization process (Nasdala et al. 2001).

Several experimental approaches (i.e., IR, Raman, neutron scattering, and proton-NMR spectroscopy) can provide information on the presence, structural environment and concentration of water in minerals. Infrared (IR) spectroscopy has become the most widely used method for detecting and quantifying even minute concentrations (i.e., as little as a few ppm H_2O) of hydrogen (Libowitzky and Beran, 2006). Additionally, polarized IR on oriented single-crystal sections offers information on the orientation of the OH dipole in the structure. Diffraction methods, such as XRD, although not sensitive to the presence of diluted structurally bound defects, can be used to provide supplementary data regarding the effect of OH incorporation on the structural parameters of the mineral host. Accordingly, the bulk of the experimental information available for the incorporation of water in zircon comes mainly from IR studies (Collett and Frondel 1953; Dawson et al. 1971; Aines and Rossman 1986; Woodhead et al. 1981; Nasdala et al. 2001; Salje and Zhang 2006; Zhang et al. 2010) with minor contribution from XRD measurements (Krstanovick 1964; Caruba et al. 1985).

The interpretation of IR spectra that suggests the presence of water in a nominally dry mineral is typically done using empirical formulas (Nakamoto et al. 1955; Novak 1974;

Libowitzky 1999), which correlate the OH stretching frequency and the O-H...O bond length. However, as pointed out by recent computational studies (Balan et al. 2011, Umemoto et al. 2011), the interpretation becomes problematic when the mechanism of water incorporation is achieved through a coupled substitution that introduces an additional local relaxation in the structure. The additional local relaxation cannot be measured by diffraction methods, which depend upon long-range order and probe the average structural sites of the major elements in a structure.This is certainly the situation for zircon, which displays only one unique oxygen position but a large number of OH stretching bands (see Table 2 in Woodhead et al. 1991), suggesting various O-H…O bond lengths and orientations.

The incorporation of H into the zircon structure can occur by several coupled substitution mechanisms (i.e., $H^{+} + M^{3+} = Si^{4+}$ and $H^{+} + M^{3+} = Zr^{4+}$) or additionally via a complex hydrogarnet-type substitution (i.e., $4H^{+} = Si^{4+}$). However the local relaxation introduced in the structure by such substitution mechanisms remains unaccounted for and leads to highly speculative interpretations of the IR data.

As a result, despite the large number of studies by IR and Raman spectroscopy, polarized IR combined with heating and deuteration, thermogravimetric, chemical and X-ray analysis, the understanding of the hydrogen locations in zircon is still ambiguous (Nasdala et al. 2001). The difficulty in understanding the locations of H in zircon, as well as the controlling effect of the incorporation mechanisms, arise from the difficulty of reconciling the IR data, which are a measure of the O-H…O bond distances (Libowitzky, 1999), with the structural data of zircon as determined by diffraction methods.

Consequently, the aim of the present paper is to evaluate the locations of H in the zircon structure by means of *ab initio* calculations and to address the role of different substitution mechanisms on the local relaxation of the structure and the resulting OH vibrational frequency.

COMPUTATIONAL PROCEDURE

Calculations were performed using the supercell approach and hybrid density functional methods as implemented in CRYSTAL09 (Dovesi et al. 2006).The performance of three hybrid HartreeFock (HF)/DFT functionals (i.e., B3LYP, B3PW and PBE0) was evaluated for the best description of the vibrational properties of the investigated defects as compared to experimental data. The three selected hybrid functionals have been extensively and successfully used for solids and have proven to generate results superior to the ones obtained from LDA or GGA approximations (Demichelis et al. 2010; Demichelis et al. 2011).Moreover, Demichellis et al. (2010) showed that for a correct description of systems containing H atoms, it is essential to include a percentage of exact HF exchange.

We adopted an all-electron basis sets formerly tested in solid state calculations and used in a previous *ab initio* study on zircon (Li and Pan 2011). The Zr basis set is Dovesi's [1s4sp3d] basis set contracted from (26s17p9d). The Si basis set is 8-41G** contracted from (20s13p2d) (Pisani et al. 1992) and the O basis set is 6-31G* with standard contraction of [3s2p1d] (Gatti et al. 1994). For calculations of the H-compensated defects, we used 85-11G* Al basis set (Catti et al. 1994), [5s4p3d] Y basis set contracted from (26s17p10d) (Towler 1995), 86-52G* Ti basis set (Muscat 1999) and 5-11G* basis set for H (Dovesi et al. 1983).

In order to minimize possible defect-defect interactions, a supercell model was used for calculating the geometry and electronic properties of the H-compensating defects. Our previous calculations on structurally similar defects (i.e., $[AlO_4/H]^0$, Botis and Pan 2009, and $[AlO_6/H]^0$,

Botis and Pan 2011) showed that a supercell size above 48 atoms was suitable for accurately describing systems with no observed defect-defect interaction. Therefore, a 2x2x2 $ZrSiO_4$ supercell containing 96 atoms was employed as a starting point for all defect calculations.

Parameters for Coulomb and HF exchange series accuracy were set to 10^{-7} and 10^{-14} Hartree with a tight accuracy on the self-consistent field energy set to $10^{-9}$and 10^{-10} for geometry optimization and anharmonic frequency calculation. A high accuracy extra-large grid (XLGRID) consisting of 75 radial and 974 angular points was employed. This grid is recommended for calculations that include heavy atoms and evaluation of properties derived from the numerical integration of energy. The Pack-Monkhorst shrink factor (Monkhorstand Pack 1976) for optimization of the unit cell was set to 8 while for calculations of the defect structures in supercells containing 96 atoms, the shrink factor was reduced to 4.

For the calculated OH stretching modes where anharmonicity effects can be as large as 200 cm^{-1}, the anharmonic stretching frequency has been evaluated. The theoretical details regarding the treatment of the OH anharmonicity have been previously discussed in detail (Tosoni et al. 2005; Merawa et al. 2003; Merawa et al. 2004). To briefly summarize, the computational procedure consists of: 1) treatment of the OH distance as a pure normal coordinate decoupled from the other vibration modes; 2) evaluation of the system's energy for a set of OH values around the equilibrium position (-0.2/+0.3 Å) and interpolation of the results by a 6^{th} order polynomial; 3) the one-dimensional nuclear Schrodinger equation is then solved using the algorithm proposed by Lindberg (1988) and (Pascale et al. 2004). This simplified approach is valid for uncoupled and non-dispersive modes, such as the OH stretching modes. In zircon the OH stretching modes are not coupled with the vibrational modes of the structure, their

frequencies being several times higher than the lattice vibrations, and the interaction of the H with the rest of the structure occurs only through weak hydrogen bonds.

RESULTS AND DISCUSSION

Bulk zircon $ZrSiO_4$ structure

Zircon has a high symmetry, $I4_1/amd$, with a structural unit of alternating edge-sharing SiO_4 tetrahedra and ZrO_8 dodecahedra (Figure 1). The chains of alternating polyhedra are parallel to the *c*-axis and are joined laterally by edge-sharing dodecahedra. While the positions of the Zr and Si atoms are constrained by symmetry (i.e., (0, 3/4, 1/8) and (0, 1/4, 3/8)), the O atoms are located at the 16*h* Wyckoff sites (0, y, z). The structure can thus be fully described by the unit cell constants *a* and *c* along with the positional parameters that define the position of the oxygen atoms (Table 1).

The unit cell parameters and fractional coordinates have been optimized using three hybrid functionals: B3LYP, B3PW, PBE0, and the equilibrium geometries have been obtained by a full relaxation of the structure (Table 1). The tested hybrid functionals perform exceptionally well at reproducing the experimentally reported values (Robertson et al. 1971), with a maximum discrepancy of 2%. Such agreement is sufficient to confidently use the selected basis sets and functionals to further study the structural details of H incorporation in zircon.

H incorporation in zircon

Several mechanisms have been proposed for the incorporation of H into crystalline zircon. The most exhaustive review of the existing experimental data accompanied by an extensive model of substitution mechanisms and possible locations of H atoms in the zircon

structure has been provided by Nasdala et al. (2001). Following the model proposed by Nasdala et al. (2001), we have investigated three main incorporation mechanisms and their effects on the H location, local structural relaxation and resulting OH vibrational frequencies.

The three investigated mechanisms, discussed in detailin the following sections are:

1. Hydrogarnet substitution: $4(OH)^{-} = (SiO_4)^{4-}$
2. H-compensated trivalent substitution at the Si site : $M^{3+} + H^{+} = Si^{4+}$
3. H-compensated trivalent substitution at the Zr site : $M^{3+} + H^{+} = Zr^{4+}$

Hydrogarnet substitution mechanism

The hydrogarnet-type substitution was originally proposed by Frondel and Collet (1957) as the main mechanism for water incorporation into zircon. Caruba et al. (1985) have reported synthetic zircon samples with 81% of the Si replaced by hydroxyl groups, and they linked the presence of the 3515 cm^{-1} OH stretching band to the hydrogarnet substitution mechanism. However, the 3500-3515 cm^{-1} band occurs rarely and with a low intensity in natural zircon (Dawson et al. 1971; Woodhead et al. 1991; Ilchenko 1994), which leads to the conclusion that although possible, hydrogarnet substitution is not an energetically favored incorporation mechanism. Alternatively, Nasdala et al. (2001) proposed a partial hydrogarnet-type substitution (i.e., Si vacancy substituted by two H atoms) as a more probable incorporation mechanism and proposed it as being responsible for the 3420 cm^{-1} (E//c) OH stretching. However, a partial-hydrogarnet defect leads to a charge imbalance, and an additional 2+ charge compensator would be necessary, either locally or remotely, which would impose supplementary energetic constrains on the system.

For the present *ab initio* investigation, we constructed a 2x2x2 $ZrSiO_4$ supercell of 96 atoms and chose one Si atom located near the center of the supercell as the incorporation site of the hydrogarnet-type defect. Two different hydrogarnet configurations were evaluated. The first configuration was constructed by removing a Si atom and inserting four H atoms, placed 1 Å from each of the remaining oxygens and aligned on the previously existing Si-O directions. The second evaluated configuration was based on the model proposed by Umemoto et al. (2011) for hydrogarnet incorporation in forsterite (i.e. one of the H atoms was placed outside of the tetrahedron while the other three H atoms were placed on the tetrahedral edges). The defective structures were then allowed to relax towards a minimum energy configuration. Comparing the ground state energy of the relaxed structures it appears that the configuration in which one of the H atoms is located outside the tetrahedron is energetically unfavorable (i.e. ΔE=6.5 eV) and it was therefore disregarded as a potential hydrogarnet geometry.

The energetically favorable hydrogarnet structure is depicted in Figure 2, and the details of the local relaxation are explicitly listed in Table 2. Using the (H…O) and (O…O) distances obtained after the structural relaxation and the correlation function of Libowitzky (1999), we calculated the corresponding vibration frequencies ω_{01}(H…O) and ω_{01}(O…O) (Table 2). The vibrational frequencies derived from Libowitzky's correlation function are located between 3400-3450 cm^{-1}. Given that the O-H…O angle is 152°, close to the critical angle of 150° that divides H bonds between bent and straight (Libowitzky, 1999) more confidence can be assigned to the frequencies that are calculated based on the relaxed H…O distances. This would result in corresponding vibration frequencies located between 3402 and 3422 cm^{-1}. Alternatively, if anharmonicity effects are considered, the *ab initio* calculated OH stretching frequencies appear to also correspond to the experimentally observed band at 3420 cm^{-1} (Nasdala et al. 2001).

The calculated OH vibration frequency for hydrogarnet is lower than the experimental frequency of 3515 cm^{-1} assigned by Caruba et al. (1985) and Nasdala et al. (2001) to the complete hydrogarnet substitution. However, Caruba et al. (1985) synthesized the H-rich zircon samples in a fluorinated environment, and it is not clear whether the 3515 cm^{-1} band represents a true hydrogarnet substitution, given the coupled nature of H^+ and F^-. The presently calculated OH stretching frequency seems to agree better with the experimentally observed 3420 cm^{-1} band, which was assigned (Nasdala et al. 2001) to a partial hydrogarnet substitution with only 2 H atoms located ata vacant Si position. Nevertheless, a discrepancy exists between the polarization of the 3420 cm^{-1}observed IR band and the theoretically calculated OH orientation. While the experimental band is polarized parallel to *c*-axis, the calculated OH bonds that belong to the hydrogarnet defect structure make a ~ 48° angle with the *c*-axis. This orientation would result in an IR band polarized, such as the ratio of the parallel to perpendicular intensities $I_{\perp}/I_{//}$=1.6 (Bekisli et al. 2012).

In order to understand the possible structural differences between a complete hydrogarnet substitution and a partial one, we evaluated several geometries for a partial hydrogarnet mechanism. After the removal of one Si atom, 2 H atoms were placed at 1 Å distance from two of the remaining O atoms, and the structure was allowed to relax towards a minimum energy configuration. Charge compensation was attained through a computational artifice by using a uniformly-distributed background of positive charge (i.e., jellium).

The relaxed structure of the partial hydrogarnet defect is depicted in Figure 2c and Figure 2d. The two H atoms, which form the partial hydrogarnet defect, bond to two O and form H…O pseudo-bonds with the remaining two O atoms. The newly formed OH bonds make angles of 30° with the *c*-axis. Following relaxation, the remaining dangling O atoms (Figure 2d) are displaced

from their original positions and form a peroxy-type bond of 1.5 Å. Although the orientation of the newly formed OH bonds is not parallel to *c*-axis, the smaller angle formed with the vertical gives rise to a polarized OH stretching band, such that the ratio of the intensities would be $I_{\perp}=6I_{//}$ (Bekisli et al. 2012). In order to obtain OH bonds that are aligned parallel to the *c*-axis, in a hydrogarnet or partial hydrogarnet-type configuration, the local relaxation of the structure would cause an extreme distortion of the Si-vacant tetrahedron. The distorted structure would be as close as possible to a vertically oriented square (i.e., bottom O atoms located directly bellow the top O atoms, at identical x and y positions). In the present *ab initio* calculations however, we did not observe such a severe distortion of the relaxed structure. Based on our results, we infer that a hydrogarnet or partial hydrogarnet substitution would display an IR signature located at ~3420 cm^{-1}, polarized such as $I_{\perp}=1.6I_{//}$ for hydrogarnet and $I_{\perp}=6I_{//}$ for partial hydrogarnet substitutions.

We note the peculiar relaxation of the partial hydrogarnet structure and the formation of the peroxy-type bond with a typical bond distance d(O-O)=1.5 Å. Although never mentioned in the literature as a potential defect in zircon, the O-O stretching vibration associated with a peroxy-type bond would be located at ~ 700-950 cm^{-1} (Budinger et al. 1984; Vacque et al. 1997; Haller et al. 1996). Such vibration frequencies (i.e., 827, 887, 934, 957 cm^{-1}) have been previously observed in Pb-irradiated zircon samples (Zhang et al. 2008), but their assignment remained a matter of debate. According to these results, the stretching vibration of a peroxy-type bond formed as a result of Pb^{2+} incorporation in zircon and charge compensated by a partial hydrogarnet substitution could be the source of the vibration bands at ~ 800 cm^{-1}.

H-compensated trivalent substitution at the Si site

253 H incorporation in zircon can also be attained through a trivalent cation substitution at the
254 Si^{4+} site. In this case H^{+} provides for charge-balance. Due to the similarity in size and abundance,
255 Al^{3+} is one of the main candidates for a trivalent substitution at the Si site.

256 Here we describe a substitution mechanism that results in an [AlO_4/H] defect as revealed
257 by *ab initio* level calculations, with particular consideration for the defect structure and OH
258 vibration frequencies. Starting from a perfect supercell structure, a Si atom was replaced by Al,
259 and a H atom was inserted at the center of one of the square channels running parallel to *c*-axis
260 and adjacent to the substituted Al. After complete relaxation of the structure, the compensating H
261 atom was located 0.98 Å from one of the O atoms belonging to the AlO_4 tetrahedron (Figure 3a
262 and b). The calculated O…H and O…O distances that correspond to the relaxed defect geometry
263 (Figure 3) are reported in Table 3. The OH stretching frequencies obtained employing
264 Libowitzky's correlation function, have also been derived for direct comparison with the *ab*
265 *initio* calculated anharmonic vibration frequencies (Table 3). There is a significant relaxation of
266 the local structure as a result of Al substitution (i.e., d(O…O)=2.92 Å following relaxation *vs.*
267 3.37 Å in the ideal structure), and the OH stretching frequencies obtained based on the empirical
268 correlation function are highly overestimated. The overestimation is visible when using both
269 d(O…O) and d(H…O) for evaluation of the stretching frequencies and point towards an
270 additional mechanism for frequency reduction. From the results of the present calculations, it
271 appears that anharmonicity may play an important role in lowering the OH stretching frequencies
272 (Table 3). Therefore a moderate relaxation of the zircon structure,caused by Al incorporation, as
273 well as the consideration of the anharmonicity factors, results in an OH vibrational frequency
274 that correlates with the experimentally observed 3385 cm^{-1} IR band.

The orientation of the OH bond is perpendicular to the *c*-axis, in complete agreement with the polarization of the aforementioned IR band. Although Nasdala et al. (2001) assigned the origin of the 3385 cm^{-1} IR band to an asymmetrically bifurcated hydrogen bond of intermediate strength oriented perpendicular to the *c*-axis and bonded to an O atom belonging to an occupied tetrahedron, no such a geometry was observed in the present simulations. Moreover an asymmetrically bifurcated hydrogen bond would significantly deviate from the correlation function of Libowitzky and yield two different OH stretching frequencies. Based on the present results, we propose the [AlO_4/H] defect as the source of the 3385 cm^{-1}(E//c) OH stretching band.

H-compensated trivalent substitution at the Zr site

Another substitution mechanism that could involve H^+ incorporation as an accompanying charge compensator is the trivalent substitution at the Zr^{4+} site. Y^{3+} and REE^{3+} are known to be dominant trace elements in zircon and commonly occupy the Zr site (Caruba et al. 1995; Finch et al. 2001; Hoskin and Schaltegger, 2007). Although previous studies propose the xenotime-type substitution (i.e., $REE^{3+}+P^{5+}=Zr^{4+}+Si^{4+}$) as the preferred incorporation mechanism for Y^{3+} and REE^{3+} (Speer 1982; Finch et al. 2001), it is clear that when the P content is insufficient to attain charge balance, H^+ could play a significant role in maintaining charge neutrality. Moreover, Hinton et al. (2003) propose that H rather than P is the main charge-balancing element within the zircon structure, and its presence may not be related to metamictization alone.

Starting from these considerations, we investigated the effect of Y^{3+} and La^{3+} incorporation in the zircon structure, when charge balance was attained by H^+ compensation. We considered two distinct locations for H^+ with respect to the M^{3+} substitution site (i.e., H close and H far, see Table 4 and Figure 4), with the intention of understanding the difference between an

298 OH environment that is directly controlled by the local relaxation around the $[M^{3+}O_8]$ defect and
299 a structural environment that is affected only by the strain the defect imposes on it's second and
300 third coordination spheres. The difference in the ground state energy between the two H
301 locations has also been investigated. The two substitutional atoms (i.e., Y^{3+} and La^{3+}) have been
302 chosen due to their common occurrence in the zircon structure and for the purpose
303 ofunderstanding the effect of the substituting atom's radius (i.e., 1.019Å for Y^{3+} and 1.16 Å for
304 La^{3+}) (Shannon 1976) on local relaxation.

305 Similar to the above-mentioned computational procedure, a Zr^{4+} atom located close to the
306 center of a 96 atoms supercell was replaced by a M^{3+} atom, and a charge compensating H^+ was
307 placed at the center of a nearby channel, running parallel to the *c*-axis (i.e., H close). For the
308 second considered location, H^+ was placed in the next nearest channel, at a distance of
309 approximately 3 Å from M^{3+} (i.e., H far).

310 After complete relaxation, the H atom bonds to one of the O atoms belonging to the
311 $[MO_8]$ dodecahedron (i.e., H close) or for the second considered structure to an O atom
312 belonging to a $[ZrO_8]$ dodecahedron (i.e., H far). In both cases the resulting OH bond has a bond
313 length of 0.98 Å and is oriented perpendicular to *c*-axis (Figure 4). The resulting (H…O) and
314 (O…O) distances are reported in Table 4. As in the case of H-compensated Al defect, the OH
315 stretching frequencies obtained employing the empirical correlation formula of Libowitzky are
316 unrealistically high as compared with the experimentally reported IR frequencies. This is,
317 however, not surprising since Libowitzky mentioned cationic influences as a major source of
318 deviation from the regression line on which the empirical correlation function was based.
319 Deviations by more than 100 cm^{-1} have been reported with decreasing metal-oxygen distances in
320 the coordination sphere of the ion.

When the OH stretching frequency was calculated at the *ab initio* level however, including the effect of anharmonicity, the calculated IR bands are located at near 3200 cm^{-1}(i.e. H close) and 3100 cm^{-1} (i.e., H far) (Table 4).

When comparing the ground state energy of the two considered H locations, the H position closest to the $[M^{3+}O_8]$ dodecahedron is the most energetically favored. Although both Y^{3+} and La^{3+} substitutions with H at the edge of the defective dodecahedrons are more energetically favored, the difference in energy between H located closer or farther away is relatively small (i.e., ~ 1 eV for Y^{3+} incorporation and ~1.7 eV for La^{3+} incorporation). Considering that the present calculations are first-principle, static calculations at 0° K, the relatively small difference in energy between the two possible H locations suggests that both locations are energetically probable at room temperature. If we assume an equal distribution between H locations closer and farther away from a M^{3+} substituted zircon atom, we can estimate that the mixture of such structural configurations would result in a broad OH stretching band located at an average position. Such an average OH stretching band would be located at ~ 3175-3195 $^{-1}$ (see Table 4) and would be characterized by a large broadening (i.e., ~ 150 cm^{-1}). However if one H position is energetically preferred (i.e., possibly higher energy difference for other substitutional cations) or the diffusion of H is controlled by low temperature conditions, we expect that the band would be resolved into a doublet (i.e., two IR bands located at ~3100 cm^{-1} and closely above 3200 cm^{-1}).

Based on the comparison of these calculations with the experimentally measured IR, the H-compensated trivalent substitution at a Zr site is the structural defect responsible for generating the 3180 cm^{-1} (E⊥c) OH stretching band. The low water content of the natural zircons containing the 3180 cm^{-1} OH stretching band (Nasdala et al. 2001) can be attributed to the

possibility of a competing substitution mechanism (i.e., xenotime) that controls the incorporation of M^{3+} at the Zr^{4+} sites. Nonetheless, in P-free synthetic samples, such as those synthesized by Trail et al. (2011), the intensity of the 3199 cm^{-1} band is relatively high. Moreover, synthetic zircon samples doped with Lu (Trail et al. 2011) show a doublet formed by two broad overlapping bands located at ~3200 cm^{-1} and 3113 cm^{-1}, in complete agreement with the calculated results.

AKNOWLEDGEMENTS

We would like to thank Dr. Tony Whiters and one anonymous reviewer who have helped improve this manuscript. The work was supported by the Office of Basic Energy Sciences of the U.S. Department of Energy, through Grant No. DE-FG02-97ER45656. DFT calculations in this research has been enabled by the use of WestGrid computing resources, which are funded in part by the Canada Foundation for Innovation, Alberta Innovation and Science, BC Advanced Education, and the participating research institutions. WestGrid equipment is provided by IBM, Hewlett Packard and SGI.

REFERENCES

Aines, R.D., and Rossman, G.R. (1985) The high temperature behavior of trace hydrous components in silicate minerals, American Mineralogist, 70, 1169-1179.

Balan, E., Ingrin, J., Delattre, S., Kovacs, I., Blanchard, M. (2011) Theoretical infrared spectrum of OH-defects in forsterite. European Journal of Mineralogy, 23: 285-292.

Bekisli, F., Fowler, B., Stavola, M., Boatner, L.A., Spahr, E., Lupke, G. (2012) Bond-angles for O-H defects in SnO_2 from polarization properties of their vibrational modes, Physical Reviews B, 85, 205202-1-4.

Botis, S.M., Pan, Y. (2009) Theoretical modeling of the Al center and its precursors in stishovite, Physics and Chemistry of Minerals, 37, 119-127.

Botis, S.M., Pan, Y. (2011) Modeling of $[AlO_4/Li^+]^{(+)}$ paramagnetic defects in alpha-quartz, Canadian Journal of Physics, 89, 809-816.

Budinger, P.A., Mooney, J.R., Graselli, J.G., Fay, P.S., Gutmann, A.T. (1981) Spectra-structure correlation of alkyl peroxides, Analytical Chemistry, 53, 884-889.

Caruba, R., Baumer, A., Ganteaume, M., Iacconi, P. (1985) An experimental study of hydroxyl groups and water in synthetic and natural zircons: A model of the metamict state, American Mineralogist, 70, 1224-1231.

Catti, M., Valerio, G., Dovesi, R., Causa, M. (1994) Quantum-mechanical calculations of the solid-state equilibrium MgO + alpha-Al2O3 MgAl2O4 (spinel) versus pressure, Physical Review B 49, 14179-14187.

Coleman, R.G., and Erd, R.C. (1961) Hydrozircon from the Wind River Formation, Wyoming, Journal of Research of the U.S. Geological Survey, 256, 297-300.

Delattre, S., Utsunomiya, S., Ewing, R.C., Boeglin, J.-L., Braun, J.-J., Balan E., Calas, G. (2007) Dissolution of radiation-damaged zircon in lateritic soils, American Mineralogist 92, 1978-1989.

Dovesi, R., Ermondi, E., Ferrero, E., Pisani, C.,Roetti, C. (1983) Hartree-Fock study of lithium hydride with the use of a polarizable basis set, Physical Review B 29, 3591-3600.

Dovesi, R., Orlando, R. (1994) Convergence properties of the supercell approach in the study of defects in solids. Phase Transitions, 52, 151-167.

Dovesi, R., Saunders, V.R., Roetti, C., Orlando, R., Zicovich-Wilson, C.M., Pascale, F., Civalleri, B., Doll, K., Harrison, I.J., Bush, I.J., D'Arco, Ph., Llunell, M. (2006) CRYSTAL06 User's Manual, University of Torini, Torino, Italy.

Dovesi, R. (2006) CRYSTAL, http://www.crystal.unito.it/Basis_Sets/zirconium.html.

Ewing, R.C. (1999) Nuclear waste forms for actinides. Proceedings of National Academy of Science, 96, 3432-3439.

Ewing, R.C. (2001) The design and evaluation of nuclear-waste forms: clues from mineralogy, Canadian Mineralogist, 39, 697-715.

Finch, R.J., Hanchar, J.M., Hoskin, P.W.O., Burns, P. (2001) Rare-earth elements in synthetic zircon: Part 2. A single-crystal X-ray study of xenotime substitution, American Mineralogist, 86, 681-689.

Frondel, C. (1953) Hydroxyl substitution in thorite and zircon. American Mineralogist, 38, 1007-1018.

Frondel, C., and Collette, R.L. (1957) Hydrothermal synthesis of zircon, thorite and huttonite. American Mineralogist, 42, 759-765.

Gatti, C., Saunders, V.R., Roetti, C. (1994) Crystal-field effects on the topological properties of the electron-density in molecular-crystals.The case of urea, Journal of Chemistry and Physics 101, 10686-10696.

Haller, K., Lunsford, J.H., Laane, J. (1996) Temperature dependence of the Raman spectrum of barium peroxide, journal of Physical Chemistry, 100, 551-555.

Hinton, R., MacDonald, R., Macgarvie, D., Tindle, A., Harley, S. (2003) The possible role of hydrogen in the substitution of rare earth elements into zircon. EGS-AGU-EUG Joint Assembly, Nice, France, abstract #5968.

Hoskin, P.W.O, and Schaltter, U. (2003) The composition of zircon and igneous and metamorphic petrogenesis. Reviews in Mineralogy and Geochemistry, vol. 53, 27-62.

Krstanovic, I. (1964) X-ray investigation of zircon crystals containing OH groups. American Mineralogist, 49, 1146-1148.

Merawa, M., Civalleri, B., Ugliengo, P., Noel, Y. and Lichanot, A. (2003) Structural, electronic and vibrational properties of $Sr(OH)_2$, calculated with different Hamiltonians. Journal of Chemical Physics, 119:1045-1052.

Merawa, M., Labeguerie, P., Ugliengo, P., Doll, K. and Dovesi, R. (2004) The structural, electronic and vibrational properties of LiOH and NaOH: an ab initio study. Chemical Physics Letters, 387:453-459.

Mumpton, F.A., and Roy, R. (1961) Hydrothermal stability and studies of the zircon-thoritegroup.Geochemica et GeocosmicaActa, 21, 217-238.

Nada, R., Nicholas, J.B., McCarthy, M.I., Hess, A.C. (1996) Basis sets for ab initio periodic Hartree-Fock studies of zeolite/adsorbate interactions: He, Ne, and Ar in silica sodalite.International Journal of Quantum Chemistry 60, 809-820.

Nakamoto, K., Margoshes, M., Rundle, R.E. (1955) Stretching frequencies as a function of the distances in hydrogen bonds. Journal of the American Chemical Society, 77, 6480-6488.

Nasdala, L., Beran, A., Libowitzky, E., Wolf, D. (2001) The incorporation of hydroxyl groups and molecular water in natural zircon ($ZrSiO_4$). American Journal of Science, 301, 831-857.

Novak, A. (1974) Hydrogen bonding in solids. Correlation of spectroscopy and crystallographic data. Structure and bonding, 18, 177-216.

Pascale, F., Tosoni, S., Zicovich-Wilson, C., Ugliengo, P., Orlando, R., Dovesi, R. (2004) Vibrational spectrum of brucite, Mg(OH)2: a periodic ab initio quantum mechanical calculation including OH anharmonicity, Chemical Physics Letters, 396, 308-315.

Rossman, G.R. (2006) Analytical methods for measuring water in nominallyanhydrous minerals In H. Keppler and J.R. Smyth, Eds., Water in NominallyAnhydrous Minerals, 62, p. 1–28. Reviews in Mineralogy and Geochemistry,Mineralogical Society of America, Chantilly, Virginia.

Salje, E.K.H., and Zhang, M. (2006) Hydrous species in ceramics for the incapsulation of nuclear waste: OH in zircon. Journal of Physics: Condenssed Matter, 18, L277-L281.

Shannon, R.D. (1976) Revised Effective Ionic Radii and Systematic Studies of Interatomic Distances in Halides and Chalcogenides, ActaCrystalographica,A32751-767

Spear, J.A. (1980) Zircon. In P.H. Ribbe, Ed. Orthosilicates, 67-112. Reviews in Mineralogy, Vol.5, Mineralogical Society of America, Washington, D.C.

Tosoni, F., Pascale, P., Ugliengo, P., Orlando, R., Saunders, R., Dovesi, R. (2005) Quantum mechanical calculation of the OH vibrational frequency in crystalline solids, Molecular Physics, 103: 2549-2558.

Trail, D., Thomas, J.B., Watson, E.B. (2011) The incorporation of hydroxyl into zircon, American Mineralogist, 96: 60-67.

K. Umemoto, R.M., Wentzcovitch, M.M., Hirschmann, D.L., Kohlstedt and A.C. Withers (2011) A first-principles investigation of hydrous defects and IR frequencies in forsterite: The case for Si vacancies. American Mineralogist, 96: 1471-1479.

Vacque, V., Sombret, B., Huvenne, J.P.,Legrand, P., Suc, S., (1997) Characterization of the O-O peroxide bond by vibrational spectroscopy, SpectrochimicaActa. Part A, Molecular and biomolecular spectroscopy, 53, 55-56.

Zhang, M., Boatner, L.A.,Salje, E.K.H., Ewing, R., Daniel, P., Weber, W.J., Zhang, Y., Farnan, I. (2008) Micro-Raman and micro-infrared spectroscopic studies of Pb- and Au-irradiated $ZrSiO_4$ Optical properties, structural damage and amorphisation, Physical Review B, 77, 144110.

Zhang, M., Salje, E.K.H., Ewing, R. (2010) OH species, U ions, CO/CO_2 in thermally annealed metamict zircon (ZrSiO4). American Mineralogist, 95, 1717-1724.

Woodhead, J.A.,Rossman, G.R., Thomas, A.P. (1991) Hydrous species in zircon. American Mineralogist, 76, 1533-1546.

FIGURE CAPTIONS

Figure 1: Bulk structure of crystalline zircon viewed: a) along the *c*-axis, onto the (001) plane defined by the *a* and *b* axes. b) A view of the zircon structure along the *a*-axis, perpendicular to

the (100) plane. The distance between oxygen atoms that are considered potential docking sites for H are marked.

Figure 2: H incorporation into the zircon structure through hydrogarnet and partial hydrogarnet substitution mechanisms: a) A view of the hydrogarnet-type defect along the *c*-axis. b) Detailed view of the hydrogarnet defect oriented in a (001) plane perpendicular to the *c*-axis. The angle made by the OH bond with the *c*-axis is ~ 48°. c) Partial hydrogarnet viewed along the *c*-axis. d) Detailed view of the partial hydrogarnet oriented in the (001) plane perpendicular to *c*-axis. Local relaxation of the structure gives rise to an O-O peroxy bond of 1.5 Å. The angle made by the OH bonds with the *c*-axis is ~ 30°.

Figure 3: H incorporation into the zircon structure as a charge compensating mechanism for trivalent substitution at the Al site. Structure of the calculated [AlO_4/H] defect in zircon viewed: a) along the *c*-axis and b) from the (001) plane perpendicular to the *c*-axis.

Figure 4: H incorporation into the zircon structure as a charge compensating mechanism forthe trivalent substitution at the Zr site. Structure of the calculated [$M^{3+}O_8$/H] defect, where M=Y and La viewed along the *c*-axis for two possible H locations: a) [$M^{3+}O_8$/H] – H close, c) [$M^{3+}O_8$/H] - H far. Detailed view of the same defect structure in an orientation perpendicular to c-axis: b) [$M^{3+}O_8$/H] – H close, d) [$M^{3+}O_8$/H] - H far.

Table 1: Calculated structural parameters for $ZrSiO_4$ compared to the experimental values of [1]Robinson et al. 1971.

	This work			Expt.[1]
	B3LYP	B3PW	PBE0	
Volume				
V (Å^3)	133.2	131.5	130.9	131
Lattice parameters				
a (Å)	6.647	6.621	6.614	6.607
c (Å)	6.029	5.996	5.988	5.982
y	0.067	0.066	0.066	0.066
z	0.194	0.193	0.193	0.195
Interatomic distances				
Si-O (Å)	1.633	1.629	1.627	1.622
Zr-O (Å)	2.149	2.138	2.135	2.131
	2.277	2.264	2.261	2.268
Zr-Si (Å)	3.015	3.000	2.994	2.991
	3.344	3.635	3.630	3.626

Table 2: Calculated (H…O) and (O…O) distances for the hydrogarnet-type defect in zircon and their corresponding OH stretching frequencies as derived from the empirical correlations of *Libowitzky (1999). $\omega_{01}$are the *ab initio* calculated OH stretching frequencies (corrected for anharmonicity) and $\omega_e\chi_e$ are the corresponding anharmonic constants.

Functional	d(H…O) Å	d(O…O) Å	Frequency (cm^{-1})*		Calculated	Anharmonic ct.
			ω_{01}(H…O)	ω_{01}(O…O)	ω_{01} (cm^{-1})	$\omega_e\chi_e$ (cm^{-1})
Full hydrogarnet (4H)						
B3LYP	1.929	2.826	3408.72	3436.62	3418.6	116.0
	1.930	2.827	3409.13	3436.97	3418.6	115.9
	1.928	2.826	3407.88	3436.15	3417.9	116.1
	1.928	2.826	3407.67	3436.03	3417.8	116.1
B3PW	1.942	2.839	3421.83	3451.15	3412.4	116.0
	1.942	2.839	3422.21	3451.41	3412.5	115.9
	1.941	2.839	3420.89	3450.60	3411.6	116.1
	1.941	2.839	3420.68	3450.46	3411.5	116.2
PBE0	1.923	2.820	3402.40	3428.92	3418.9	117.6
	1.923	2.820	3402.68	3429.10	3419.2	117.6
	1.923	2.820	3402.27	3428.80	3419.0	117.6
	1.923	2.820	3402.29	3428.78	3419.0	117.6
Partial hydrogarnet (2H)						
B3LYP	1.761	2.725	3142.72	3258.53	3426.5	113.9
	1.735	2.699	3079.22	3185.80	3426.7	113.9
B3PW	1.747	2.712	3111.15	3223.26	3429.3	111.7
	1.706	2.672	3001.03	3091.04	3429.2	111.7
PBE0	1.742	2.705	3099.20	3203.84	3416.7	116.3
	1.706	2.669	3000.29	3081.97	3416.4	116.3

Table 3: Calculated (H…O) and (O…O) distances for the [AlO_4/H] defect in zircon and their corresponding OH stretching frequencies as derived from the empirical correlations of *Libowitzky (1999). $\omega_{01}$are the *ab initio* calculated OH stretching frequencies (corrected for anharmonicity) and $\omega_e\chi_e$ are the corresponding anharmonic constants.

Functional	d(H…O) Å	d(O…O) Å	Frequency (cm^{-1})*		Calculated	Anharmonic ct.
			ω_{01}(H…O)	ω_{01}(O…O)	ω_{01} (cm^{-1})	$\omega_e\chi_e$ (cm^{-1})
[AlO_4/H]						
B3LYP	2.000	2.967	3472.141	3538.525	3383.5	107.5
B3PW	2.184	3.121	3564.008	3575.266	3342.1	114.8
PBE0	1.951	2.920	3430.782	3515.849	3384.7	108.2

Table 4: Calculated (H…O) and (O…O) distances for the [YO_8/H] and [LaO_8/H] defects in zircon and their corresponding OH stretching frequencies as derived from the empirical correlations of *Libowitzky (1999). $\omega_{01}$are the *ab initio* calculated OH stretching frequencies (corrected for anharmonicity) and $\omega_e\chi_e$ are the corresponding anharmonic constants.

Functional	d(H…O) Å	d(O…O) Å	Frequency (cm^{-1})*		Calculated	Anharmonic ct.
			ω_{01}(H…O)	ω_{01}(O…O)	ω_{01} (cm^{-1})	$\omega_e\chi_e$ (cm^{-1})
[YO_8/H] – H close						
B3LYP	1.959	2.929	3437.475	3520.594	3269.0	119.1
B3PW	1.905	2.881	3382.574	3488.996	3252.5	111.6
PBE0	1.904	2.878	3380.579	3486.702	3269.5	120.2
[YO_8/H] – H far						
B3LYP	1.913	2.885	3391.455	3492.302	3122.2	112.0
B3PW	1.864	2.841	3329.670	3452.643	3099.0	113.6
PBE0	1.862	2.837	3327.052	3449.345	3128.4	111.9
[LaO_8/H] - H close						
B3LYP	1.951	2.923	3430.538	3517.044	3220.1	130.3
B3PW	1.897	2.871	3372.919	3481.659	3198.9	132.7
PBE0	1.894	2.869	3369.346	3480.035	3219.6	131.2
[LaO_8/H] - H far						
B3LYP	1.863	2.838	3328.272	3449.604	3110.2	112.7
B3PW	1.818	2.797	3256.556	3397.811	3086.7	114.3
PBE0	1.814	2.792	3250.863	3391.310	3116.1	112.7

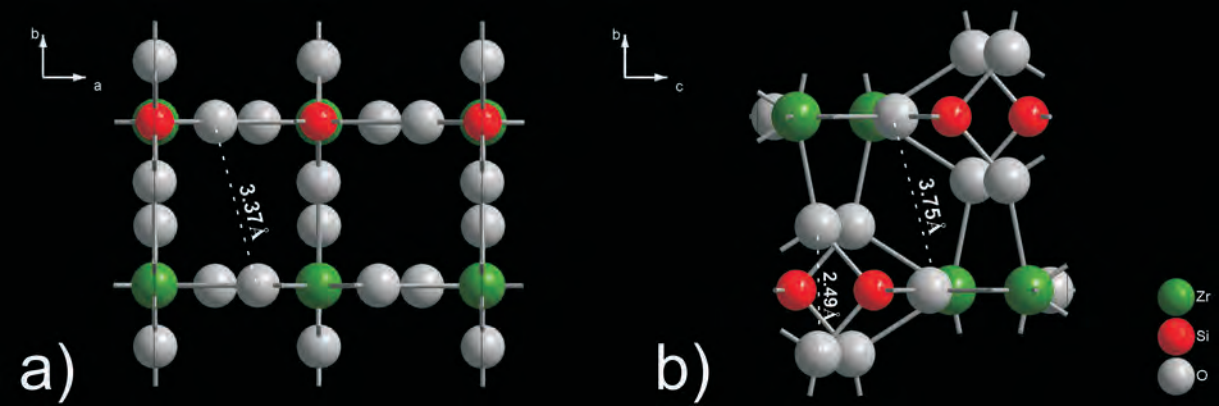
b
a
3.37 Å
a)
b
c
3.75 Å
2.49 Å
b)
Zr
Si
O

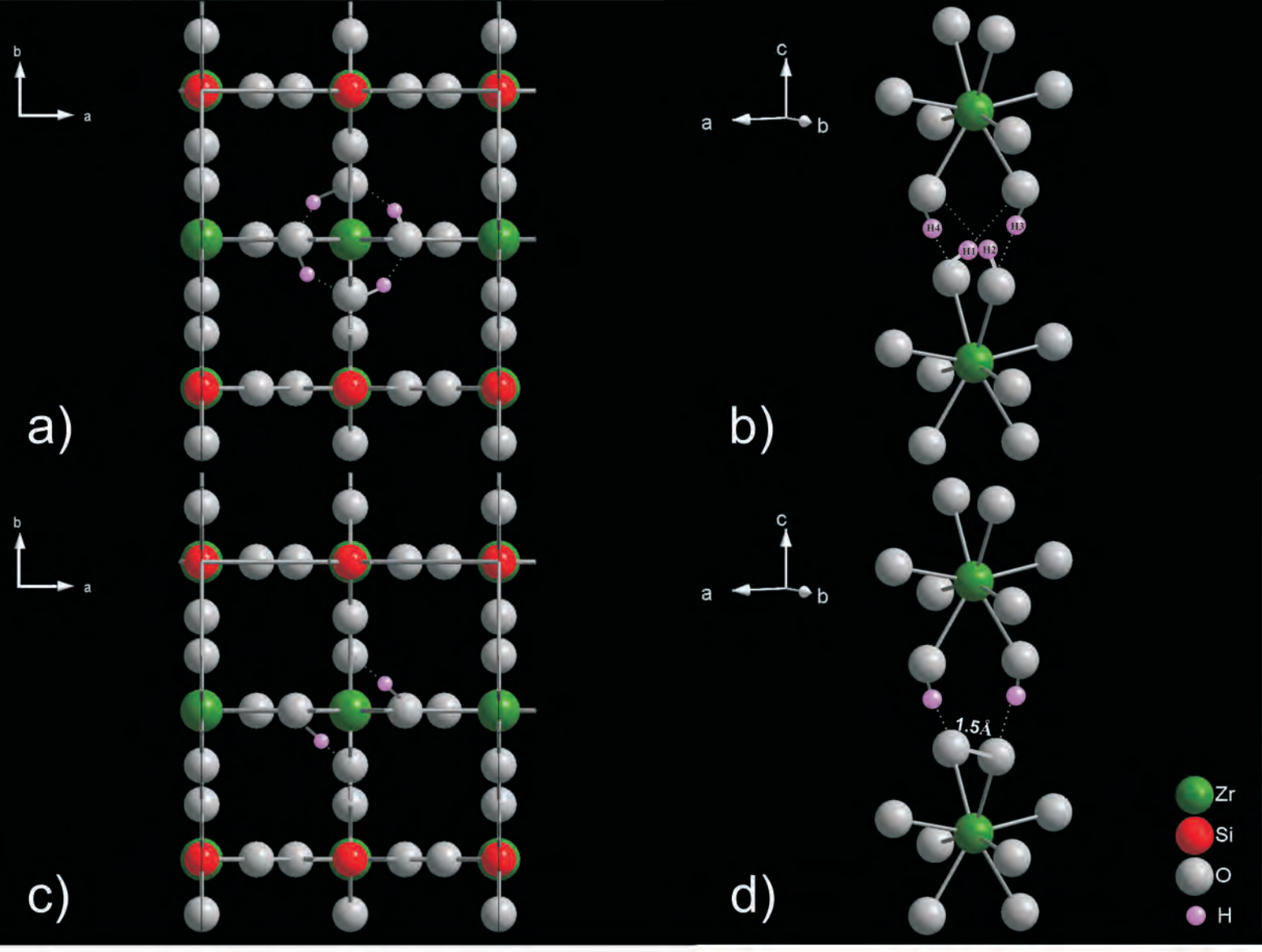
b
a
a)
b
a
c
b)
H4
H3
H1
H2
b
a
c)
c
a
b
1.5Å
d)
Zr
Si
O
H

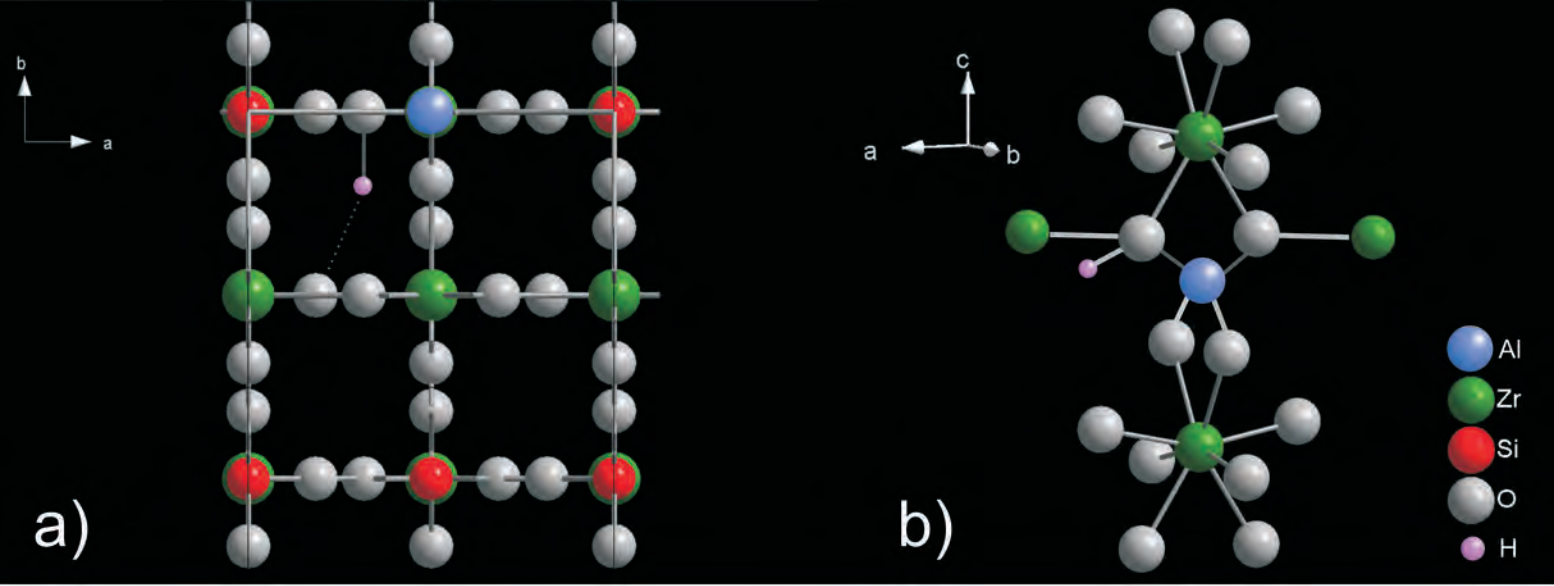
b
a
a)
c
a
b
b)
Al
Zr
Si
O
H

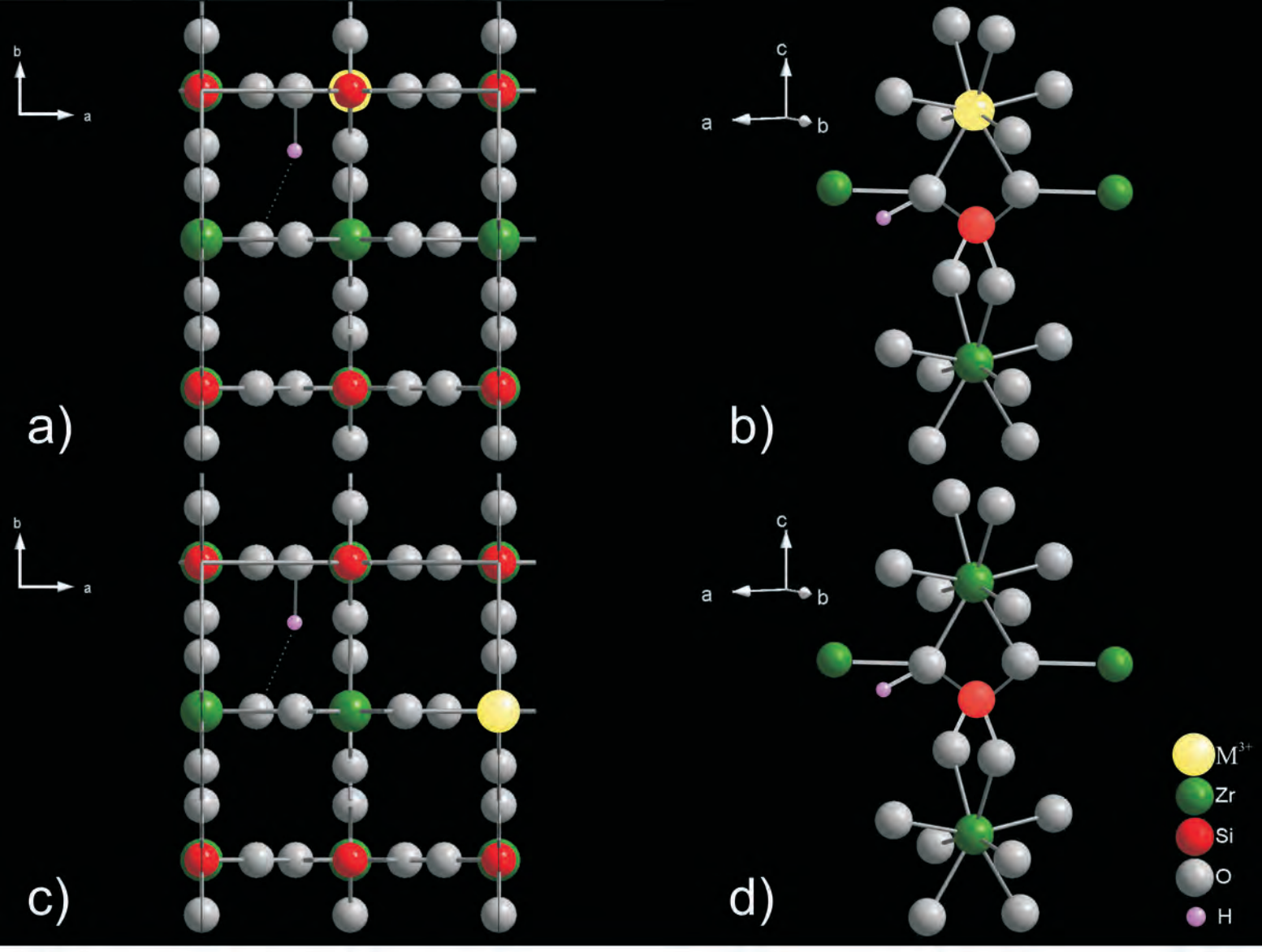
b
a
a)
b
a
c
b)
b
a
c)
c
a
b
d)
M3+
Zr
Si
O
H